Distribution of water masses and glacial meltwater on the continental shelf near the Totten Glacier

Alessandro Silvano[1,2], Stephen R. Rintoul[2,3], Beatriz Peña-Molino[3] and Guy D. Williams[1,3,4]

[1] Institute for Marine and Antarctic Studies, University of Tasmania, Hobart, TAS, Australia
[2] CSIRO Marine and Atmospheric Research, Hobart, TAS, Australia.
[3] Antarctic Climate and Ecosystems Cooperative Research Centre, University of Tasmania, Hobart, TAS, Australia.
[4] Antarctic Research Council Centre of Excellence for Climate System Science, University of New South Wales, Sydney, NSW, Australia, 2052

Corresponding author: Alessandro Silvano (Alessandro.Silvano@utas.edu.au)

Key Points:

- Warm (>0°C) modified Circumpolar Deep Water is widespread on the continental shelf, overlaid by fresh Winter Water
- Two deep troughs allow relatively warm water to reach the ice-shelf cavities and drive basal melt
- Freshening by addition of glacial meltwater is extensive at mid-depths on the inner shelf

Abstract

Warm waters flood the continental shelf on the Amundsen and Bellingshausen seas in West Antarctica, driving thinning of several outlet glaciers through rapid melting of their ice shelves. On the contrary, waters on the continental shelf in East Antarctica are cooler and ice shelves experience relatively low rates of basal melt. An exception is provided by the Totten and Moscow University ice shelves on the Sabrina Coast, where basal melt rates are comparable to West Antarctica. Recent oceanographic observations have revealed that relatively warm (~-0.4°C) modified Circumpolar Deep Water (mCDW) intrudes beneath the Totten Ice Shelf through a 1100 m trough, delivering enough heat to explain the rapid basal melt. Here we use observations from a recent summer survey to show that warm (up to 0.3°C) mCDW is widespread on the Sabrina Coast continental shelf in the bottom layer overlaid by fresh (salinity~34.3) Winter Water. Dense Shelf Water is not observed. A 1000 m trough allows water at -1.3°C to reach the Moscow University ice-shelf cavity to drive basal melt. Freshening by addition of glacial meltwater is widespread on the southern shelf at depths above 300-400 m, with peaks in meltwater concentrations up to 4-5 ml l^{-1} concentrated in fresh outflows from the ice-shelf cavities. Our observations indicate that the ocean properties on the Sabrina Coast more resemble those found on the continental shelf of West Antarctica than those typical of East Antarctica.

1. Introduction

The Antarctic Ice Sheet flows toward the coast through several outlet glaciers. Floating ice shelves form where an outlet glacier reaches the ocean. Back stresses produced by flowing ice shelves along side-walls and topographic rises can restrain ("buttress") the glacial flow into the ocean [*Dupont and Alley,* 2005]. A thinning or collapse of the buttressing ice shelves would reduce the restraint on the glacial flow, increasing the ice discharge into the ocean. Accelaration during the last few decades in the flow of some of the outlet glaciers has led to a dramatic increase in Antarctic ice loss, with most of the ice discharge occurring along the coast of the Amundsen and Bellingshausen seas in West Antarctica [*Rignot et al.,* 2008; *Harig and Simons,* 2015; *Wouters et al.,* 2015]. Here, the ice loss has been primarily attributed to thinning of the buttressing ice shelves as a result of rapid basal melt by ocean heat flux [*Shepherd et al.,* 2004; *Pritchard et al.,* 2012].

The ocean heat flux in West Antarctica is associated with intrusions of warm (>0 °C), salty (>34.5) and slightly modified Circumpolar Deep Water (mCDW) onto the continental shelf. This warm water fills the bottom layer and is able to access the cavity of several ice shelves to drive rapid basal melt [*Jenkins and Jacobs,* 2008; *Jacobs et al.,* 2011; *Dutrieux et al.,* 2014; *Jacobs et al.,* 2013]. Winter convection does not extend to sufficient depth to destratify the water column and erode the mCDW in these regions, resulting in a shallow mixed layer overlying the warm mCDW [*Petty et al.,* 2013].

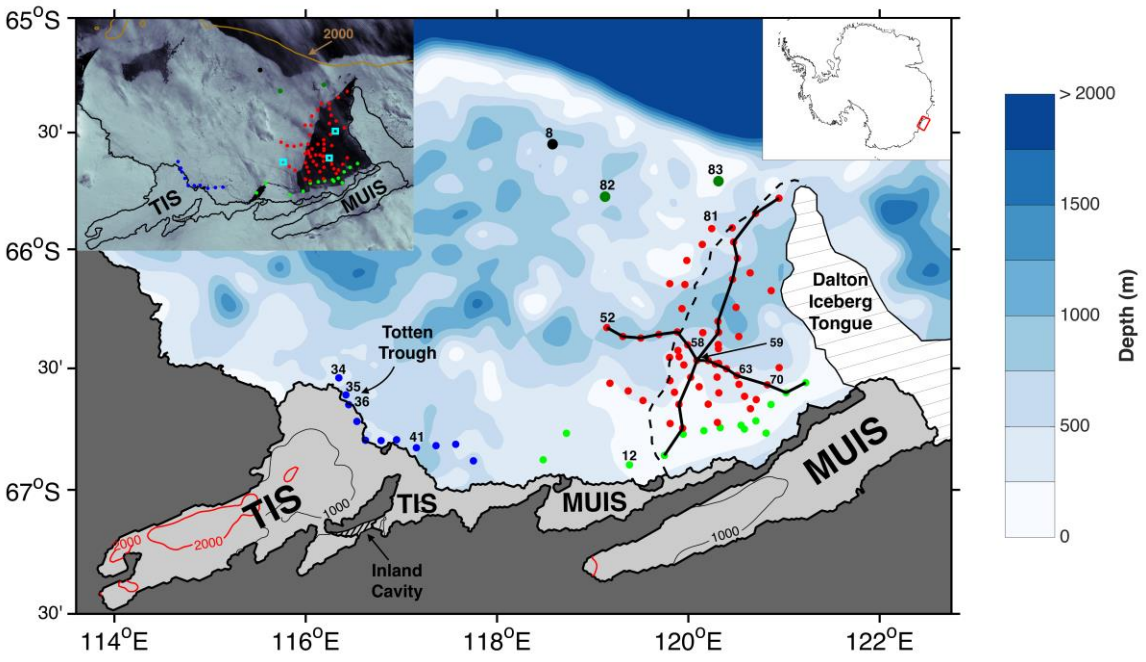

Figure1. Map of the survey area. Overlaid is the bathymetry and the coastline [Bedmap2, *Fretwell et al.,* 2013]. Bathymetry from geophysical data beneath the Totten Ice Shelf (TIS) is included [*Greenbaum et al.,* 2015]. Red, green and blue dots indicate the stations collected in the Dalton Polynya (DP), in proximity to the Moscow University Ice Shelf (MUIS) and TIS calving fronts, respectively. The location of stations 82 and 83 from BROKE are shown in dark green, while station 8 from SIPEX is shown in black. The dashed area indicates the inland cavity identified by *Greenbaum et al.* [2015], while the Totten Trough is highlighted near station 35 and 36. The dashed white area north of the MUIS is the Dalton Iceberg Tongue, a combination of grounded icebergs and fast ice. The black lines highlight the two transects shown in Figure 2 and 3. The dashed line indicates the approximate eastern boundary of the area covered by sea ice. Stations shown in Figure 5-6-8-10-11 are labelled. In the inset on the upper-left corner is a MODIS [*Scambos et al.,* 1996] image (22 January 2015) with coastline overlaid. Light blue squares are the location of the moorings, while the brown line is the 2000 m isobath which shows the approximate location of the contintental slope.

In many other parts of Antarctica, active coastal polynyas drive strong convection in winter. Polynyas are regions of enhanced sea-ice formation, where water masses are transformed by local processes such as atmospheric cooling, wind stress and brine rejection. In the strongest polynyas, the wintertime convection from sea-ice formation is

104 sufficient to overturn the entire water column to produce cold (~ surface freezing point)
105 and saline (> 34.5) Dense Shelf Water (DSW). Because of its high density, DSW sinks to
106 the bottom mixing with other water masses including, if present, mCDW. Examples of
107 strong polynyas are found in the Ross Sea [*Jacobs et al.,* 1970], in the Weddell Sea [*Gill*,
108 1973] and in several areas in East Antarctica, such as the Adélie Coast [*Rintoul*, 1998],
109 Vincennes Bay [*Kitade et al.,* 2014] and Prydz Bay/Cape Darnley [*Williams et al.*, 2016;
110 *Ohshima et al.*, 2013]. DSW formed in these regions overflows the shelf break and
111 cascades down the slope, mixing with ambient water to form Antarctic Bottom Water,
112 thus contributing to the global overturning circulation [*Johnson*, 2008; *Marshall and*
113 *Speer*, 2012]. Part of the DSW produced in these polynyas is able to access the cavities of
114 nearby ice shelves. Since the continental shelf usually gets deeper toward the grounding
115 line of an ice shelf, DSW is steered along isobaths to reach the deepest areas near the
116 grounding line [*Jacobs et al.,* 1992]. The depression of the seawater freezing point with
117 increasing pressure, ~ 0.75°C every 1000 dbar [*Foldvik and Kvinge,* 1974], implies that
118 the DSW is warmer than the local freezing point and therefore able to melt the base of the
119 ice shelf near deep grounding lines.
120 East Antarctic ice shelves located in regions where cold DSW is formed (e.g. the
121 Mertz Glacier Tongue on the Adélie Coast or the Amery Ice Shelf in Prydz Bay)
122 experience low area-averaged rates of basal melt (< 2 m $year^{-1}$) compared to the
123 Amundsen and Bellingshausen seas (> 10 m $year^{-1}$) [*Rignot et al.,* 2013; *Depoorter et al.,*
124 2013; *Liu et al.,* 2015]. However, an exception is provided by ice shelves located on the
125 Sabrina Coast, namely the Totten and Moscow University ice shelves (TIS and MUIS,
126 respectively, Figure 1), which show rates of basal melt comparable with those observed

127 in the Amundsen and Bellingshausen seas.

128 TIS and MUIS represent the floating end of the Totten and Moscow University
129 glaciers, respectively. These glaciers drain a large sector of the marine-based Aurora
130 Subglacial Basin and their stability is crucial for the future Antarctic contribution to the
131 global sea level due to the large amount of ice stored in this sector of the East Antarctic
132 Ice Sheet [*Sun et al.,* 2016]. The Totten Glacier alone drains a volume of ice equivalent to
133 3.5 m of sea-level rise, an amount similar to the entire West Antarctic Ice Sheet
134 [*Greenbaum et al.,* 2015]. Two recent studies show that the grounded part of the Totten
135 Glacier has experienced sustained mass loss (6.8±2.4 Gt yr^{-1}) and thinning (0.7±0.1 m yr^{-1})
136 during the past two decades [*Li et al.,* 2015; *Li et al.,* 2016]. Satellite estimates suggest
137 that the TIS has experienced periods of thinning and thickening, with no significant trend
138 during the past 20 years [*Paolo et al.*, 2015]. Ocean modelling studies suggest that
139 mCDW is able to access the TIS cavity to drive rapid basal melt [*Khazendar et al.,* 2013;
140 *Gwyther et al*., 2014]. Their results indicate that the thermal forcing of such intrusions is
141 tightly linked to the activity of the Dalton Polynya (DP) east of the TIS (Figure 1). When
142 sea-ice production is higher than the average, cold water formed in the polynya mixes
143 with the mCDW that intrudes onto the continental shelf weakening its properties. When
144 the production is lower, mCDW reaches the TIS cavity in a less modified form and drives
145 more basal melt, possibly triggering a thinning of the Totten Glacier.

146 A snapshot of the oceanographic conditions observed during the austral summer
147 of 2015 at the calving front of the TIS indicates that a deep trough, the Totten Trough
148 (see Figure 1), allows relatively warm (~-0.4°C) mCDW to reach the cavity [*Rintoul et*
149 *al.,* 2016]. The associated heat flux is sufficient to sustain a basal melt rate over 10 m yr^{-}

150 [1], in agreement with satellite observations [*Rignot et al.*, 2013; *Depoorter et al.*, 2013;
151 *Liu et al.*, 2015]. Other measurements collected on the outer continental shelf show the
152 presence of warm mCDW near the seafloor in summer and late winter below 400-500 m,
153 and no evidence of DSW [*Bindoff et al.*, 2000; *Williams et al.*, 2011]. However, it is not
154 known whether polynya activity is sufficient to form DSW and/or modify the properties
155 of the mCDW.

156 Here we use an extended dataset to that described in *Rintoul et al.* [2016]. We
157 show that mCDW is widespread on the continental shelf at depths below 500 m. Fresh
158 (salinity ~ 34.3) Winter Water overlies the saline mCDW. We also provide evidence that
159 deep and relatively warm water is the main source of basal melt not only of the TIS, as
160 shown in *Rintoul et al.* [2016], but also of the MUIS. Buoyant and fresh outflows driven
161 by basal melt are found along the TIS and MUIS calving fronts. Freshening by addition
162 of glacial meltwater is not restriced to these outflows, where the meltwater concentrations
163 rises to 4-5 ml l^{-1}, but is widespread on the southern shelf at depths shallower than 300-
164 400 m. Finally, a comparison with other shelves around Antarctica shows that ocean
165 properties on the Sabrina Coast (fresh Winter Water overlying warm mCDW, absence of
166 DSW, and substantial input of glacial meltwater) are more similar to those found in West
167 Antarctica than conditions typical of East Antarctica.
168
169
170
171
172

2. Data

A survey was conducted on the inner shelf of the Sabrina Coast (115°E – 125°E) on the RV *Aurora Australis* (AU1402) between December 23 2014 and January 6 2015 (Figure 1). We show the results from the analysis of 81 CTD stations collected during this expedition (Figure 1). CTD data include continuous profiles of temperature (°C), salinity (PSS78), pressure (dbar) and dissolved oxygen ($\mu mol\ l^{-1}$). Data were vertically averaged in 2-dbar bins with calibration performed using bottle samples [*Rosenberg and Rintoul,* 2016]. Uncertainties on the measurements of temperature, salinity and pressure are ~ 0.001°C, 0.002 (PSS78) and 1 dbar, respectively. The relative uncertainty on the dissolved oxygen data is ~ 1%. Temperature and salinity data from a year-long mooring deployment on the shelf (see the inset in Figure 1 for location) indicate decorrelation time scales of about 30 days on average, with minimum values exceeding two weeks, confirming the synopticity of the survey.

In our analysis we include data collected in two previous surveys on the continental shelf of the Sabrina Coast. Two CTD stations were occupied in austral summer 1996 during BROKE (Baseline Research on Oceanography Krill and the Environment) [*Bindoff et al.,* 2000] (Figure 1). Temperature from a single ice station in late winter 2007 during SIPEX (Sea Ice Physics and Ecosystem eXperiment) is also used [*Williams et al.,* 2011] (Figure 1). Measurements of temperature, salinity and dissolved oxygen from the Adélie Coast in East Antarctica and from Pine Island Bay in West Antarctica are also discussed in our work. Data from the Adélie Coast were collected during the AU1402 voyage after the survey of the Sabrina Coast, while measurements from Pine Island Bay were collected in austral summer 2009 [*Jacobs et al.,* 2011].

3. Results

3.1. Water Mass Classification

A meridional section in the DP reveals four water masses present on the shelf (Figure 2). Relatively warm and salty mCDW is found near the sea floor. The σ_θ = 27.7 kg m^{-3} isopycnal is chosen to define the upper boundary of mCDW. (As neutral density is not well defined in regions where few data are available, as on the continental shelf of the Sabrina Coast, we use surfaces of potential density anomaly referenced to the surface, σ_θ, to define different layers). The mCDW is the densest water mass found on the shelf during the survey; no DSW was observed.

A homogeneous layer of remnant Winter Water (WW), a product of wintertime convection, lies above the mCDW. The WW temperature is close to the surface freezing point (~-1.8°C). A thin, warmer summer surface layer of Antarctic Surface Water (AASW) overlies the WW. The σ_θ = 27.55 kg m^{-3} surface appears to be a reasonable boundary between WW and AASW (Figure 2). However, in order to capture the water mass that is the product of winter convection, excluding water from the seasonal and main pycnocline, we restrict our definition of WW to subsurface water in the σ_θ range 27.55 to 27.7 kg m^{-3} and potential temperature range -1.75 to -1.92°C.

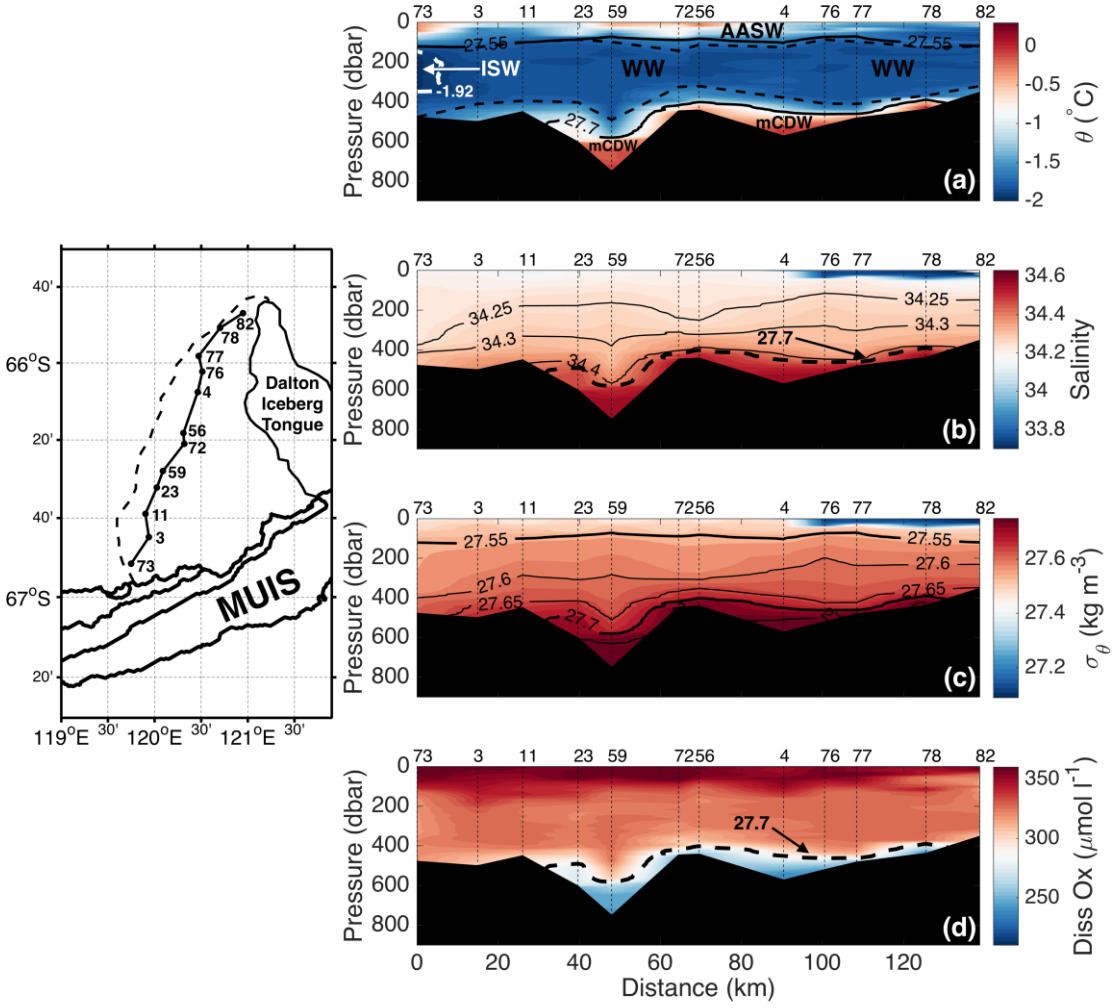

Figure 2. Meridional Section. (a) Potential temperature θ, (b) salinity, (c) potential density σ_θ and (d) dissolved oxygen section from the meridional transect through the Dalton Polynya shown in Figure 1 and highlighted in the lateral inset (the dashed black line is the approximate eastern boundary of the area covered by sea ice). CTD stations are indicated by the vertical dashed lines (numbered along the top of the plot). In panel (a) contours of σ_θ are included in black as well as the contour of θ = -1.92°C (Ice Shelf Water) in dashed white, while the black dashed lines indicate the top and the bottom of the Winter Water (WW) layer. The modified Circumpolar Deep Water (mCDW) is found below the contour of σ_θ = 27.7 kg m^{-3} (dashed black line in the panel (b) and (c)) and the Antarctic Surface Water (AASW) above the contour of σ_θ = 27.55 kg m^{-3}.

The last water mass found during the survey is Ice Shelf Water (ISW), which results from mixing between glacial meltwater from ice-shelf basal melt and ambient shelf water masses. ISW is distinguished by the other water masses because its temperature is significantly colder than the surface freezing point, due to the influence of basal melting at depth. We define ISW as water colder than -1.92°C, which corresponds roughly to the local subsurface freezing point at 50 dbar; it is unlikely that water colder than this value is the result of the interaction with the atmosphere during the winter [*Orsi and Wiederwohl,* 2009]. ISW is found near the coast (see Figure 2) in the same density range as the WW (27.55 kg $m^{-3} < \sigma_\theta <$ 27.7 kg m^{-3}). The classification of the relevant water masses found on the shelf of Sabrina Coast is summarized in Table 1.

Table 1: Classification of the water masses

Water Mass	σ_θ (kg m^{-3})	θ (°C)
AASW	$\sigma_\theta < 27.55$	
WW	$27.55 < \sigma_\theta < 27.7$	$-1.92 < \theta < -1.75$
ISW	$27.55 < \sigma_\theta < 27.7$	$\theta < -1.92$
mCDW	$\sigma_\theta > 27.7$	

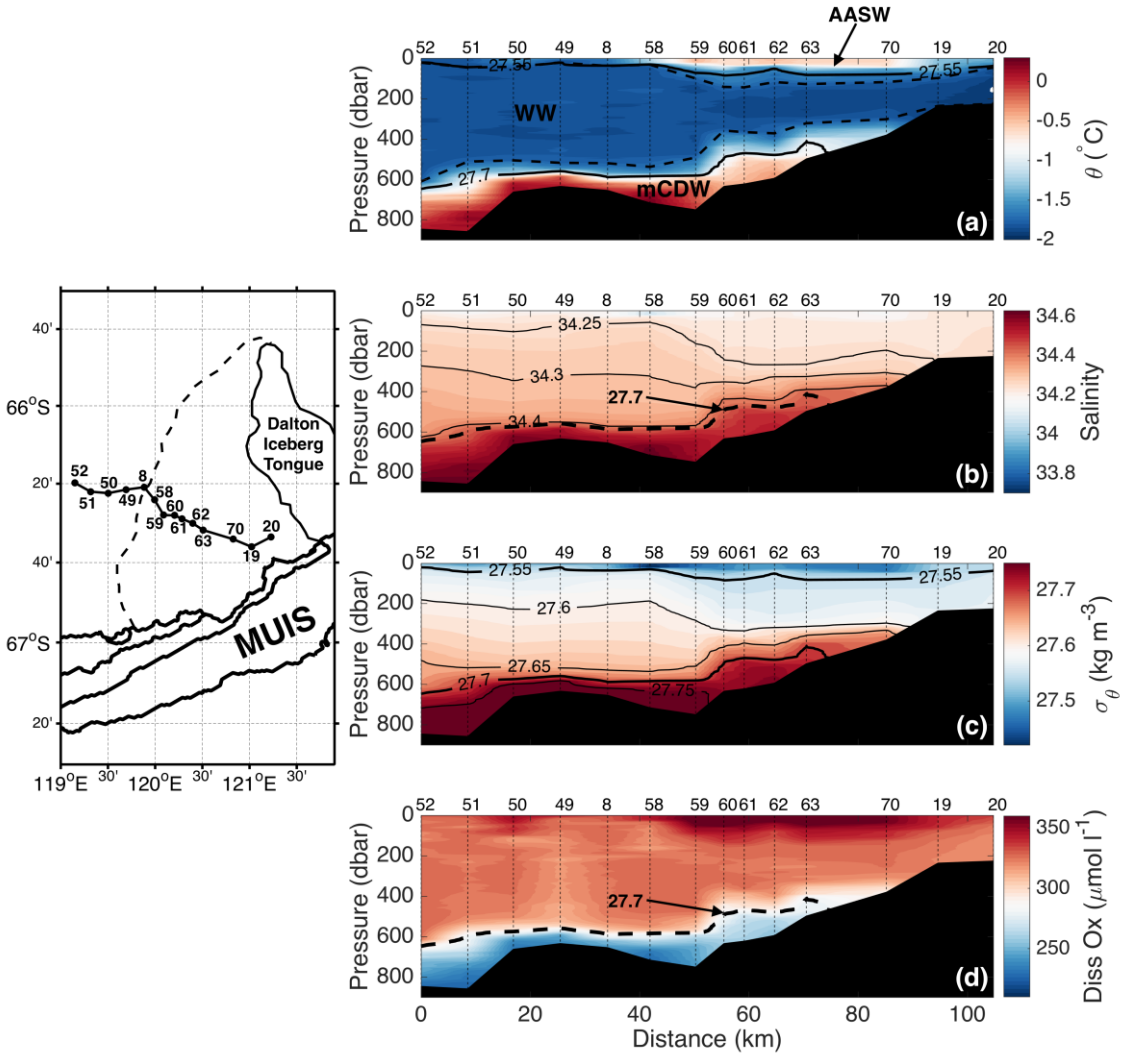

239

240 **Figure 3.** Zonal Section. As in Figure 2 but for the zonal transect shown in Figure 1 and
241 in the lateral inset.
242
243
244 **3.2. Spatial Variability**

245 We divide the domain into two main regions in order to analyze the spatial variability
246 of the water properties: the DP (red points in Figure 1) and the ice front, which includes
247 the stations closest to the TIS and MUIS calving front (blue and green points in Figure 1,
248 respectively). A recent airborne survey revealed the presence of an inland inland trough
249 that connects the main trunk of the TIS with the adjacent fringing ice shelf (dashed area

250 in Figure 1) [*Greenbaum et al.,* 2015]. In order to include this cavity in the definition of
251 the TIS, we extend the eastern boundary of this ice shelf to 118° E. We define the
252 floating ice shelves between 118° E and 122.5° E as the MUIS. Furthemore, for
253 simplicity, the DP group includes stations located in sea ice west of the actual polynya
254 and the ice-front group includes stations collected along the narrow part of the coast
255 where the ice is grounded (between the main trunk and the subsidiary part of the MUIS,
256 according to Bedmap2).
257
258 **3.2.1. Dalton Polynya**
259 Our observations show that deep mCDW is widespread on the DP and its
260 southward spreading is steered by bathymetry. The meridional transect through the DP
261 indicates that mCDW is found below 400-500 m across most of the section (Figure 2).
262 However, closer to the ice front, the deepest water gets colder as the bottom shoals. Near
263 the MUIS, the sea floor rises to about 500 m and the bottom water temperature is almost
264 at the surface freezing point. The distribution of salinity and dissolved oxygen are closely
265 related to potential temperature. Offshore the warmest mCDW is also the most saline and
266 lowest in oxygen, while closer to the ice edge, the bottom water becomes fresher and
267 higher in oxygen. A similar pattern is found in the zonal direction (Figure 3). In the
268 south-eastern sector of the polynya, mCDW is not found in the shallow waters (< 300 m)
269 near the coast. Moving north-westward, the temperature at the bottom increases as the
270 bottom deepens. At station 63, where the sea floor is about 500 m deep, the mCDW
271 signal reappears. In both transects isopycnals follow isobaths in the deep layer, implying
272 that mCDW flows according to bathymetry.

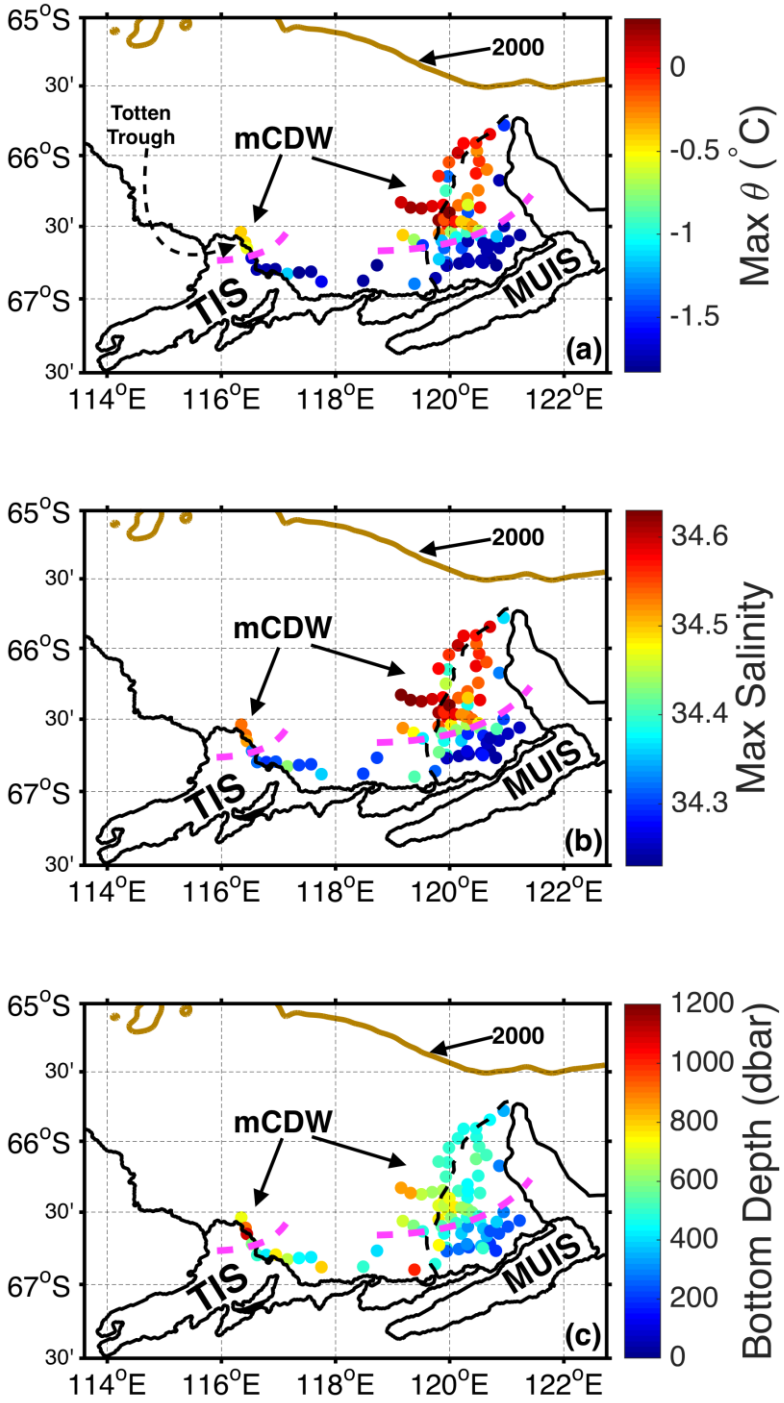

273

274 **Figure 4**. Maximum Property Values. (a) Maximum potential temperature θ and (b)
275 salinity beneath the summer mixed layer. The brown line is the 2000 isobath (showing the
276 approximate location of the continental slope) and the black dashed line the approximate
277 eastern boundary of the area covered by sea ice. The magenta dashed lines are the mCDW
278 southern boundary. (c) Bottom depth (dbar).

To help visualize the spreading of mCDW on the shelf, we show the spatial distribution of the warmest and saltiest water found beneath the summer mixed layer (Figure 4a and 4b). The warmest (0.3°C), saltiest (34.63) and lowest oxygen (~230 μmol l^{-1}, Figure 3) mCDW is located in the western sector of the DP. In the north, the mCDW is slightly cooler and fresher. As we get closer to the coast in the DP, the bottom shoals (Figure 4c) and the deep water becomes cooler and fresher. The magenta dashed line indicates the southern boundary of the mCDW core. As expected, this boundary corresponds roughly to where the bathymetry becomes shallower than 500 m. In the DP, south of this line, the bottom layer gets progressively cooler and fresher until any trace of mCDW vanishes and the WW reaches the bottom.

The mCDW layer in the polynya is characterized by strong vertical gradients: temperature and salinity increase with depth, while the oxygen content diminishes (Figure 5). The strong salinity and consequently density gradient implies that mCDW is more stable than the overlying WW (Figure 5d). The pycnocline gradient deepens from ~ 400 m in the shallower northern region to ~ 600 m in the deeper water in the west, resulting in a 100-200 m thick bottom layer in both regions (Figure 2-3) with small spatial variability of the water properties (Figure 4).

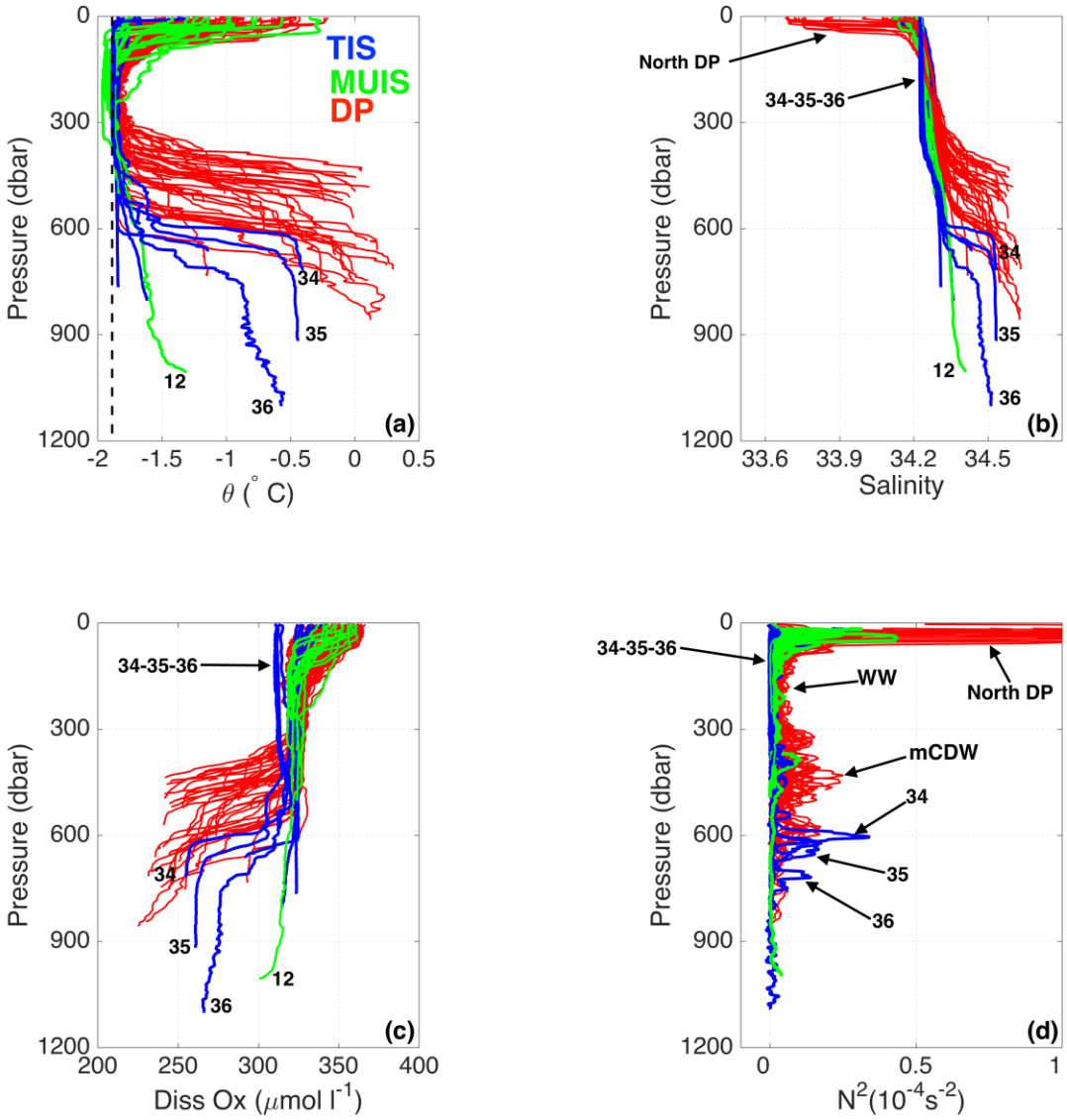

Figure 5. Vertical Profiles. (a) Potential temperature θ, (b) salinity, (c) dissolved oxygen and (d) N^2 (square of the Brunt–Väisälä frequency) profiles from DP (red), MUIS (green) and TIS (blue) calving fronts. The westernmost profiles (34-35-36) are labelled, as well as station 12 where a deep trough is found at the MUIS calving front. Overlaid in black in (a) is the surface freezing temperature profile for a salinity of 34.4, representative of the domain. N^2 has been smoothed with a vertical running mean over 20 dbar.

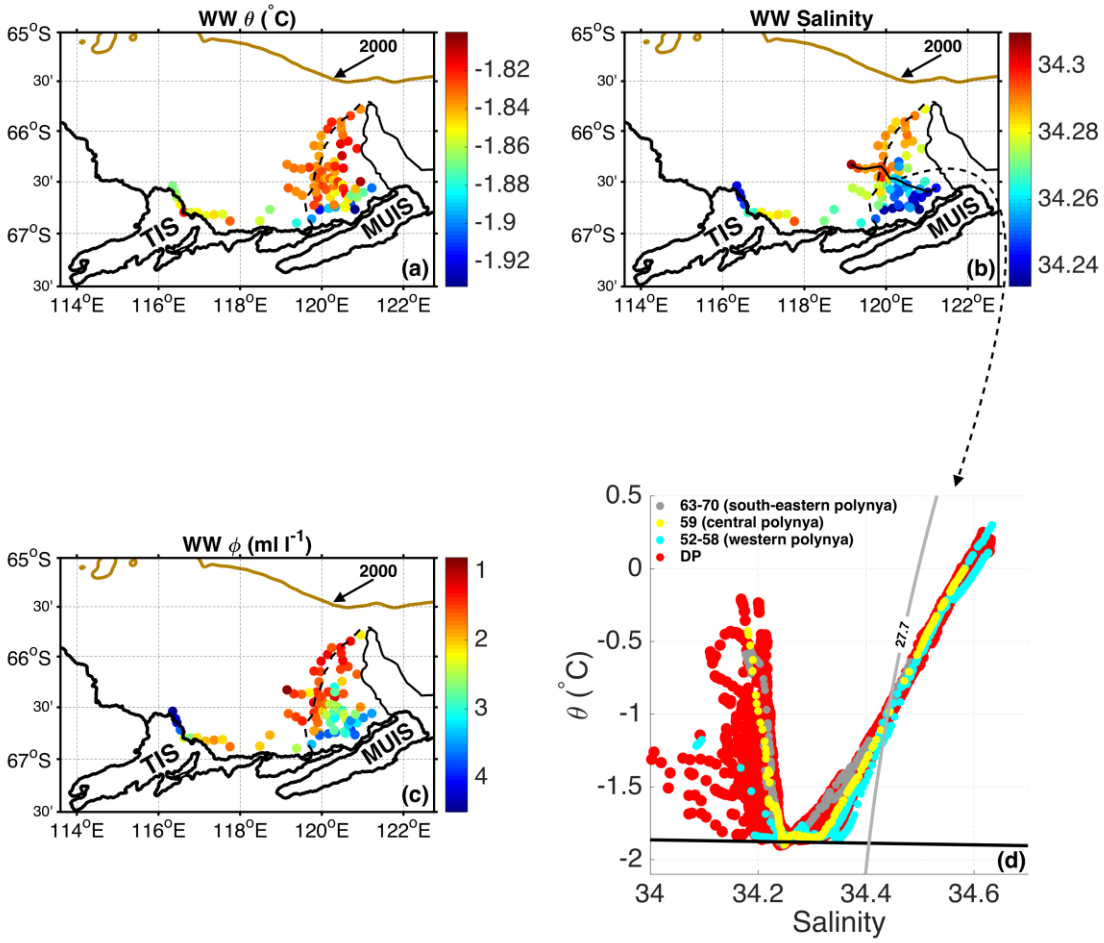

Figure 6. WW Properties. (a) Mean potential temperature θ, (b) salinity, (c) basal meltwater fraction ϕ of Winter Water, WW. The brown line indicates the 2000 m isobath (showing the approximate location of the continental slope) and the black, dashed line is the approximate eastern boundary of the area covered by sea ice. Note that the Ice Shelf Water is included in the WW properties. Note that when the WW upper limit does not overlap with the maximum depth where the ϕ estimate is contaminated by surface processes, we consider the deepest among the two surfaces as the upper boundary for the vertical average. (d) Potential temperature θ versus salinity from DP. The red points indicate data from all the profiles collected in the DP, while gray points (station 63 and 70) are indicative of the south-eastern DP, yellow points (station 59) of the central DP and the light blue points (station 52 and 58) of the western DP. These stations are chosen along the zonal transect highlighted in (b) and in Figure 3. For the exact location of these stations see Figure 1. The grey line is the contour of σ_θ = 27.7 kg m^{-3} (upper boundary of mCDW) and the black line is the surface freezing point.

Above the mCDW, the WW fills most of the water column, occupying a 300 to 500 m thick layer, depending on the bathymetry. The WW is cold (~-1.8°C), relatively fresh (salinity~34.3) and higher in oxygen (~330 μmol l^{-1}) than the underlying mCDW. In contrast to their vertical homogeneity, the WW properties show a large horizontal variability. First of all, the WW temperature near the coast is ~ 0.1°C lower than in rest of the polynya (Figure 6a, note that we included both WW and ISW in order to capture the product of the interaction between ice and ocean on intermediate waters). Moreover, the WW salinity substantially decreases approaching the coast with values up to 0.05-0.06 lower than in the western/northern polynya (Figure 6b). This gradual freshening is reflected in the downward tilting of isohalines and isopycnals toward the coast (clearly seen along the 34.25 isohaline, see Figure 2 and 3).

The shift to cooler and fresher values near the coast is not restricted to the WW layer, but also observed in the underlying pycnocline. This behavior is clearly seen by following the properties of the pycnocline on a θ-S diagram. If for example we consider the measurements taken along the zonal transect shown in Figure 3, we can see a shift of the pycnocline (mCDW-WW mixing line) toward the bottom left (cooler and fresher) corner of the diagram approaching the coast (Figure 6d). Our results therefore show that most of the water column is affected by cooling and freshening near the coast, including at a depth of 300-400 m.

Finally, the upper part of the water column is occupied by the AASW. The AASW shows strong variability across the region reflecting the absence or presence of sea ice and whether or not sea-ice melt has occurred yet. The polynya is ice free and therefore AASW is relatively warm (up to ~ -0.2°C) and occupies a ~ 50 m thick layer.

346 Outside the polynya, AASW is essentially absent and the WW layer extends to the
347 surface. It is worth mentioning that in the northern polynya we observe a fresh (salinity <
348 34) surface layer due to sea-ice melting that occurred in the last days of the survey
349 (Figure 2 and 5b). This surface layer is highly stratified ($N^2 \sim 10^{-4}\ s^{-2}$, Figure 5d) due to the
350 strong flux of freshwater at the surface. Because of the strong stratification, the observed
351 freshwater input due to melting of sea ice does not affect the underlying WW. In fact the
352 WW properties (e.g., salinity) are similar here to the western polynya, where sea-ice
353 melting did not occur (Figure 6a and 6b).
354
355 **3.2.2. Ice Front**
356 The ice-front section indicates that relatively warm (~-0.4°C), salty (~34.53) and
357 oxygen poor (~260 μmol l^{-1}) mCDW reaches the western sector of the TIS calving front
358 (Figure 7). Here the deep water is colder and fresher than the mCDW found in the DP,
359 but still 2-2.2°C above the in situ freezing temperature. Direct velocity measurements
360 from a lowered Acoustic Doppler Current Profiler (LADCP) confirm that the warm water
361 is flowing strongly into the cavity through the Totten Trough at station 35 and 36
362 [*Rintoul et al.*, 2016]. Because the warm water at depth is flowing into the cavity, the
363 interleaved layers observed at depth at station 36 (Figure 5) are a surprise. The
364 interleaving at depth might indicate mixing with a small amount of glacial meltwater that
365 detrains from the ice-shelf base at depth. Except for the interleaved layers, the mCDW at
366 the western TIS front forms a relatively homogenous deep layer (Figure 5), in contrast to
367 the well-stratified mCDW found in the DP. The homogeneity and relatively cool
368 temperature of the mCDW at the ice front likely reflects the presence of a sill that

restricts access of water warmer than - 0.4°C to the TIS cavity.

Above the mCDW layer, the θ-*S* diagram shows that the pycnocline (mCDW-WW mixing line) observed at stations 34-35-36 in the western sector of the TIS front departs substantially from the DP trend (Figure 8a). This shift toward fresher (and cooler) values is a signal of addition of freshwater. In fact, other measurements from the TIS calving front (station 41) overlap the DP trend, confirming that this shift is not due to different ambient water properties on the Sabrina Coast continental shelf, but to the addition of freshwater along the western ice front. The *O*-*S* diagram confirms the strong departure of the mCDW-WW mixing line from the ambient trend (Figure 8b).

The WW at the western TIS front is fresh (~34.25), low in oxygen (~300 μmol l^{-1}) and very weakly stratified compared to the WW found elsewhere on the shelf (Figure 5), including further east along the calving front (Figure 7). The low oxygen and salinity are responsible for the bump observed in the *O*-*S* plot (Figure 8b) and reflects an outflow driven by upwelling of a mixture of glacial meltwater and mCDW from the cavity [*Rintoul et al.,* 2016]. Further east along the TIS calving front there are no indications of any substantial fresh outflows. At the eastern TIS calving front, the deep water that can reach the inland cavity hypothesized by *Greenbaum et al.* [2015] is between the freezing point and -1.1°C (station 41 to 33, Figure 7), significantly colder than in the Totten Trough. Here *Rintoul et al.* [2016] has shown that the heat flux into the cavity is negligible compared to the Totten Trough.

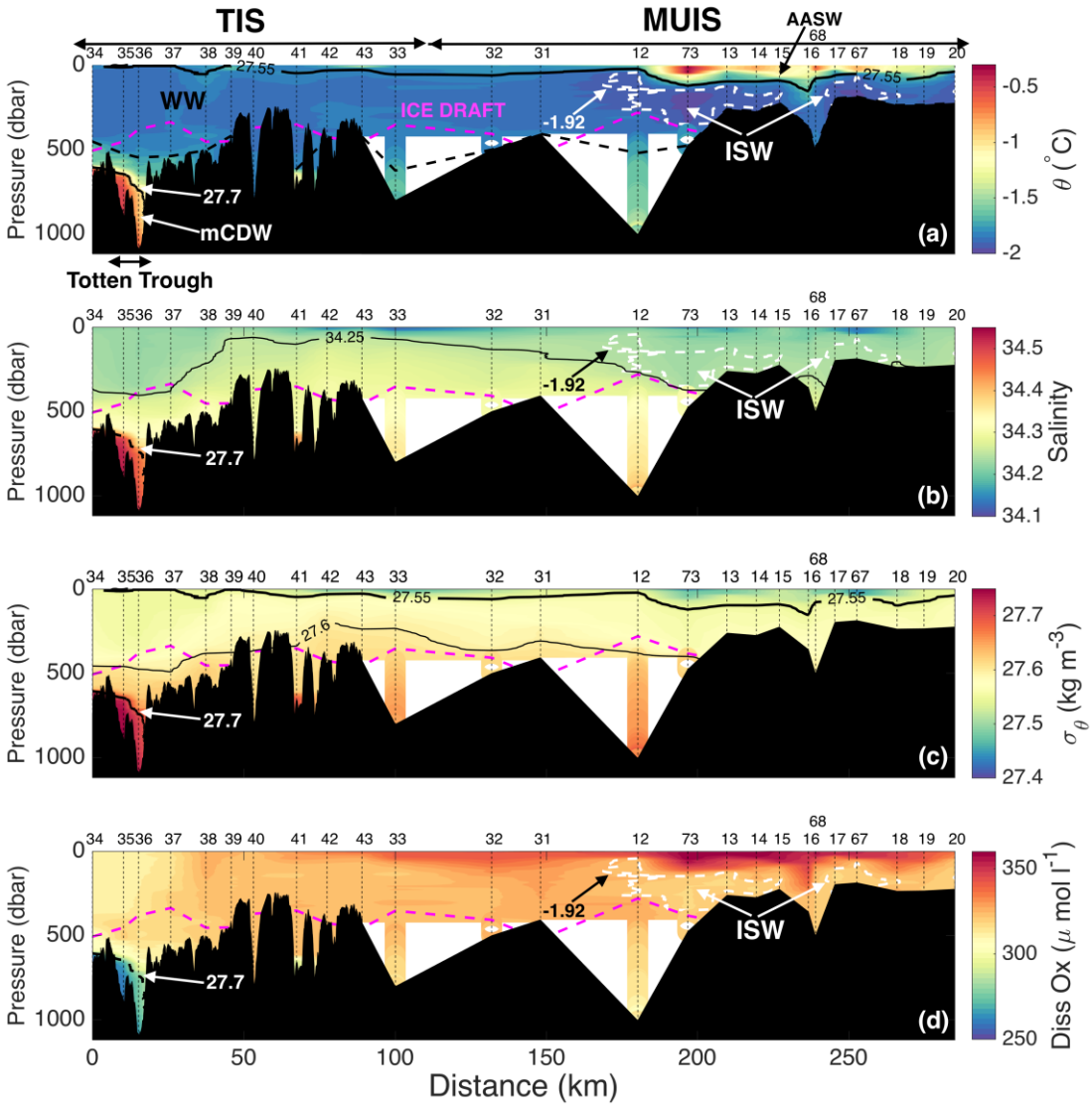

389

390 **Figure 7.** Ice-front Section. As Figure 2 but for the calving front of TIS and MUIS (blue
391 and green dots in Figure 1, respectively). Note that the upper limit of the WW layer
392 roughly overlaps the potential density contour of 27.55 kg m^{-3} and therefore is not
393 labelled. From station 34 to 43 we use the bathymetry data collected during the voyage.
394 East of station 43 the coverage does not provide high resolution bathymetry on a straight
395 line between the stations and therefore only the depth at each station is used. Along the
396 MUIS calving front, where the distances between stations are large, we do not interpolate
397 below the deepest common depth at each station pair. The magenta dashed line indicates
398 the approximate draft of the ice shelf near the calving front. From station 34 to station 42
399 the draft is interpolated from airborne measurements [*Greenbaum et al.*, 2015], while
400 from station 43 to 15 the draft is obtained from Bedmap2 estimate of ice thickness
401 [*Fretwell et al.*, 2013]. East of station of 15 the ice front is grounded, according to
402 Bedmap2.

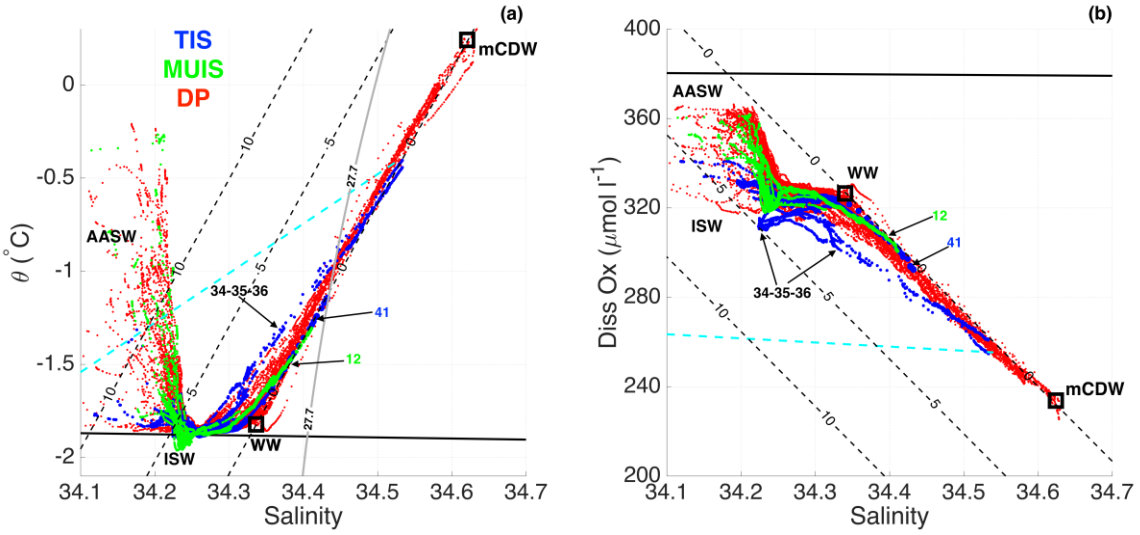

Figure 8. *θ-S/O-S* diagram. (a) Potential temperature *θ* versus salinity and (b) dissolved oxygen versus salinity from DP (red), MUIS (green) and TIS calving fronts (blue). The cyan dashed line is the mixing line (in the *θ-S* plot also known as Gade Line) between the warmest mCDW found in front of TIS and pure glacial meltwater, while the black dashed lines indicate contours of basal meltwater fraction (ml l^{-1}). The square boxes refer to the ambient properties used to calculate the basal meltwater fraction. The black line is the surface freezing point in (a) and the surface of saturation for water at the surface freezing point (b). The westernmost profiles (34-35-36) are labelled. The grey line in panel (a) represents the surface of σ_θ = 27.7 kg m^{-3} (upper boundary of mCDW). AASW = Antarctic Surface Water; ISW = Ice Shelf Water; mCDW = modified Circumpolar Deep Water; WW = Winter Water.

In contrast to the TIS, the WW reaches the bottom along most of the MUIS calving front. Only one deep (~1000 m) trough at station 12 shows relatively warm (~-1.3°C) and oxygen poor (~300 μmol l^{-1}) deep water (Figure 7). In the proximity of this trough the WW is replaced by ISW (*θ* < -1.92°C) at depths shallower than the ice draft, between 100 and 400 m below the sea surface (Figure 7). The ISW is fresher (~34.25) and lower in oxygen (~320 μmol l^{-1}) than the surrounding WW (~330 μmol l^{-1}). The ISW properties are also clear in the *θ-S* and *O-S* diagram by the bumps below the surface freezing point and below the WW-mCDW mixing line trend, respectively (Figure 8). To

summarize, we observe at the MUIS ice front relatively warm water at depth that can access the cavity through a deep trough, coincident with low-oxygen ISW at depths shallower than the ice draft. These findings indicate that the ISW results from basal melt driven by deep intrusions of relatively warm and low oxygen water into the MUIS cavity, similar to the TIS. Low oxygen ISW is not only found in front of the ice shelf, but along most of the coast where the ice is grounded, up to 75 km east of the deep trough located at station 12 (Figure 7).

3.3. Freshwater Variability

In this section we quantify the glacial meltwater concentration in the water column throughout the survey area. Glacial meltwater is produced by ice-shelf/iceberg basal melting and surface runoff. The contribution from surface runoff is negligible since summer air temperature in the interior of the East Antarctic Ice Sheet and on the Sabrina Coast is well below freezing and therefore surface melting is currently minimal [*Fyke et al.,* 2010; *Picard and Fily,* 2006]. For simplicity we will refer hereafter to glacial meltwater by ice-shelf/iceberg basal melt as basal meltwater. We use the method of *Jenkins* [1999] to estimate the basal meltwater fraction ϕ from potential temperature, salinity and dissolved oxygen. Estimates of ϕ using this technique or using other tracers as neon and helium are consistent [*Jenkins and Jacobs*, 2008; *Kim et al.,* 2016]. Indeed the method introduced by *Jenkins* [1999] has been successfully applied both at the calving front of several ice shelves [e.g. *Jenkins and Jacobs*, 2008; *Jacobs et al.,* 2011] and on the continental shelf further offshore [*Randall-Godwin et al.,* 2015].

This method allows estimation of the input of basal melt assuming that the ambient water is a mixture of two water masses. In our case, we estimate the basal meltwater fraction beneath the summer mixed layer, where the ambient water is a mixture of WW and mCDW. If two conservative properties $\chi^{1,2}$ are known, ϕ can be calculated as follows:

$$\begin{cases} \psi^{2,1} = (\chi^2 - \chi^2_{mCDW}) - (\chi^1 - \chi^1_{mCDW})\left(\frac{\chi^2_{WW} - \chi^2_{mCDW}}{\chi^1_{WW} - \chi^1_{mCDW}}\right) \\ \phi = \frac{\psi^{2,1}_{obs}}{\psi^{2,1}_{melt}} \end{cases} \qquad [1]$$

where 'obs' indicates the observed values, 'WW'/'mCDW' indicates the reference values for the end members in the ambient water, and 'melt' indicates the properties of pure glacial meltwater. Using potential temperature, salinity and dissolved oxygen as conservative properties (χ), three different estimates of ϕ can be obtained based on three possible pairs of these tracers (θ-*S,* θ-*O* and *O*-*S*). The values corresponding to the warmest, saltiest, lowest oxygen water found on the shelf (θ = 0.3°C, *S* = 34.63 and *O* = 230 μmol l^{-1}) are taken as representative of the mCDW core. The WW end member (θ = -1.8°C, *S* = 34.34 and *O* = 327 μmol l^{-1}) is defined by the saltiest WW found in the domain [*Randall-Goodwin et al.,* 2015].

The temperature of pure glacial meltwater θ_{melt} can be extrapolated from the so-called Gade Line which describes the mixing line in θ-*S* space between pure glacial meltwater and the oceanic water source [*Gade,* 1979; *Jenkins and Jacobs,* 2008]:

$$\theta_{melt} = \theta_f - \frac{L}{c_w} - \frac{c_i}{c_w}(\theta_f - T_i) \qquad [2]$$

where θ_f is the freezing point temperature at the ice-shelf base and depends on salinity and pressure; L is the latent heat of ice fusion (3.35×10^5 J kg^{-1}); c_W and c_i are the specific heat capacity of seawater and ice (4000 and 2010 J kg^{-1}C^{-1}, respectively) and, T_i is the temperature of the basal ice that we assume to be -15°C. The oceanic source can be any water parcel found along the mCDW-WW mixing line. Considering a typical ice draft in TIS of 500 m [from Bedmap2, *Fretwell et al.*, 2013] and a salinity of 34.4 representative of the domain, we find that θ_{melt} is about - 92°C, comparable to estimated values in Amundsen ice shelves [e.g., *Hellmer et al.*, 1998; *Jenkins and Jacobs*, 2008]. Note that ϕ is not very sensitive to the estimated θ_{melt} and hence to the values of the freezing point temperature or ice temperature selected.

The oxygen content of pure glacial meltwater is estimated from the empirical relation obtained by *Martinerie et al.* [1992] between oxygen concentration of the ice (and therefore of pure glacial meltwater) and the elevation where the ice is formed. According to this empirical law and considering that the elevation of the catchment that feeds the TIS and MUIS is around 2000 - 3000 m [*Fretwell et al.*, 2013], we obtain a value around 900 μmol l^{-1} for the dissolved oxygen content of pure glacial meltwater (note that ϕ is not particularly sensitive to this value). The mixing line between the warmest, saltiest and lowest oxygen mCDW found in front of TIS and pure glacial meltwater in θ-S (Gade Line) and O-S space is shown in Figure 8 by the cyan line. The aforementioned shifting of the pycnocline at the western TIS front toward the Gade Line supports the hypothesis that basal melt supplies a source of freshwater.

Following *Jenkins and Jacobs* [2008], we regard O-S as the most reliable pair to calculate ϕ. When the difference between the basal meltwater fraction calculated with the

488 other two pairs (θ-S and θ-O) is larger than 3.5 ml l^{-1}, we disregard the calculation
489 because it is likely affected by interaction with the atmosphere. Beneath this level, the
490 uncertainity in the estimated ϕ is mainly due to the deviation from linear mixing between
491 WW and mCDW [*Jenkins and Jacobs*, 2008]. In order to provide a quantitative estimate
492 of this uncertainity, we calculate the difference between ϕ estimated as described above
493 and ϕ calculated considering the freshest form of WW found on the shelf (S = 34.27). We
494 perform this calculation for every set of in situ θ, S and O. Basically we investigate the
495 impact of a shifted mixing line on the calculation of ϕ. Although this shift is not
496 observed, it provides an upper bound on the uncertainty, as it represents the maximum
497 plausible departure from the observed mixing line. Neglecting negative values of ϕ,
498 which are not physical and arise from shifting the mixing line, the average difference
499 between the two calculations is smaller than 2 ml l^{-1}. We then treat 2 ml l^{-1} as the upper
500 bound on the uncertainty of ϕ.

501 The basal meltwater fraction agrees well with the observed water properties
502 (Figure 9). Where there are inflows of deep and warm water, as in the Totten Trough and
503 in the MUIS trough at station 12, the basal meltwater content is small. On the other hand,
504 where there are fresh outflows, ϕ increases. The highest basal meltwater content is found
505 in the outflow along the western TIS calving front with values up to 5 ml l^{-1}. The ISW
506 also has a strong meltwater signature, as expected, with maximum values of ϕ up to 4 ml
507 l^{-1}.

508 The influence of the basal meltwater input is not limited to the TIS and MUIS
509 calving front. As noted above, the WW salinity decreases near the coast in the polynya
510 (Figure 6b). The basal meltwater concentration shows a similar distribution (Figure 6c).

The linear correlation between WW salinity and WW ϕ is -0.87 ($p < 0.001$), ignoring the surface layer and values of ϕ less than the estimated error of 2 ml l^{-1}. The high correlation suggests the low salinity of WW in the southern polynya reflects diluition by basal meltwater.

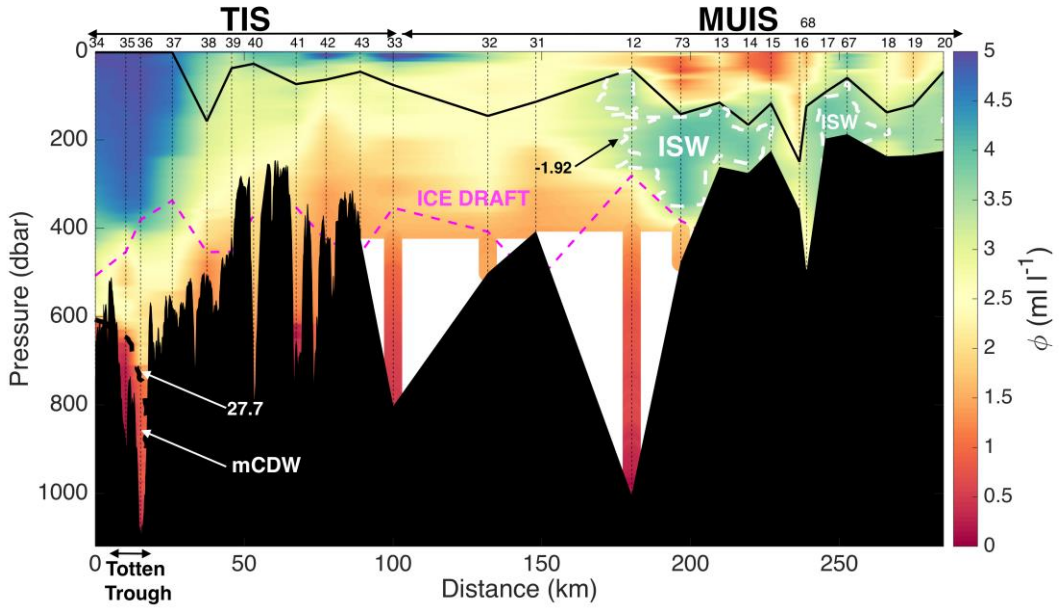

Figure 9. Basal Meltwater Fraction. Vertical section of the basal meltwater fraction ϕ (ml l^{-1}) in front of TIS and MUIS. The surface of σ_θ = 27.7 kg m^{-3} (upper boundary of mCDW) is indicated by the dashed black line, while the magenta dashed line represents the ice draft, as in Figure 7. The black line is the maximum depth where surface contamination is likely to affect the calculation of ϕ. θ = -1.92°C contours (Ice Shelf Water) are in dashed white.

4. Discussion

Our oceanographic observations show that deep and relatively warm mCDW is widespread below 500 m on the continental shelf of the Sabrina Coast. Fresh WW overlies the saline mCDW. Therefore, during the winter prior to the survey, convection on the continental shelf and in particular in the polynya was weak and the water formed not sufficiently dense to mix with the underlying mCDW. As a consequence, the

observed mCDW variability within the survey area can be explained largely in terms of bathymetry. The warmest mCDW is found in the deeper areas west of the polynya. Southward shoaling of the bottom prevented the mCDW from reaching the coast in the polynya, while relatively warm water can reach the TIS and MUIS cavity only through localized troughs. Furthermore the presence of a bathymetric barrier, such as a sill, in areas uncovered by our survey presumably prevents the warmest water found on the shelf from reaching the TIS and MUIS cavities. Excluding airborne surveys that cover only the TIS cavity and surroundings, the only available bathymetric information on the shelf of the Sabrina Coast is derived from satellite altimetry measurements [e.g., *Smith and Sandwell,* 1997], which do not resolve small-scale features such as sills or narrow troughs. Our results highlight the need for geological surveys able to provide high resolution bathymetry essential for modelling studies to reproduce and forecast intrusions of warm water beneath the TIS and MUIS.

Deep water observed at the ice front is cooler than the mCDW observed in the polynya but still about 1°C (at the MUIS) and 2°C (at the TIS) above the local freezing point and therefore sufficiently warm to produce substantial basal melt at depth and outflows of glacial meltwater. *Rintoul et al.* [2016] concluded that the warm water intrusions beneath the TIS are responsible for the rapid basal melt inferred by satellites. Using our extended dataset we conclude that the rapid basal melt observed at the MUIS is also likely driven by deep intrusions of relatively warm water.

Widespread basal meltwater in the southern DP causes the observed shoreward freshening of the water column above the mCDW. Three lines of evidence support this statement. First of all we found a strong correlation between WW salinity and WW basal

meltwater fraction in the polynya. Second, we observed a shoreward freshening of the pycnocline at 300-400 m depth, explainable only by input at depth of basal meltwater. Finally, other possible sources of freshwater come from melting of sea ice, which has been shown not to affect the water column below the thin summer mixed layer, and from precipitation, which also enters the surface layer and cannot explain the observed spatial variability in such a small domain. We then conclude that the extensive presence of basal meltwater explains the freshening of WW and pycnocline waters toward the coast of the DP, similar to what observed in the Amundsen and Bellingshausen seas, where the meltwater signature at mid-depths is widespread on the continental shelf [*Wahlin et al*., 2010; *Randall-Godwin et al*., 2015; *Zhang et al*., 2016].

The widespread influence of basal meltwater on water properties in the polynya suggests there may be multiple sources. In particular, high meltwater concentrations are observed well to the east of the outflow inferred near the deep trough at station 12, whereas we would expect meltwater to be advected to the west by the coastal current. One possible source is basal melt beneath the main trunk of the MUIS that exits the cavity at the calving front east of 121.5°E and is advected west by the coastal current. Due to the complicated structure of the coast, there could even be some undetected conduits in the grounded region between the main MUIS trunk and the DP, such as a cavity, that would serve as a pathway for the meltwater. Another possible source comes from submarine melting of icebergs packed in the Dalton Iceberg Tongue (located east of the DP, see Figure 1). However, the low oxygen ISW found in the south-eastern polynya requires melting to be primarily driven by mCDW. The shallow draft (< 500 m) of the icebergs suggest that mCDW cannot reach their submerged part. Therefore we speculate

575 that basal melt under the main trunk of the MUIS could represent a major source of the
576 basal meltwater found in the DP. If correct, this would imply that mCDW is also able to
577 access the cavity beneath the main and faster flowing trunk of the MUIS, as also
578 suggested by modelling studies [*Khazendar et al.*, 2013; *Gwyther et al*., 2014].
579 A comparison with data collected during BROKE and SIPEX reveals that
580 conditions observed in the polynya in 2015 were similar to those found on the outer shelf
581 in 1996 and 2007 (Figure 10). In each year warm and saline mCDW was present near the
582 sea floor, overlaid by cold and fresh WW. The salinity measurements from SIPEX in late
583 winter 2007 presented a large offset (>0.1) and therefore are not reported here. However,
584 the vertical structure indicates that the WW in 2007 was about 0.3 lower in salinity than
585 the underlying mCDW [*Williams et al.*, 2011], similar to what observed in 1996 and
586 2015. Satellite estimates indicate that sea-ice production in the DP is lower than in other
587 major polynyas (e.g. Mertz or Ross polynyas) and that interannual variability is relatively
588 small [*Tamura et al.*, 2016; *Williams et al.*, 2011]. Several lines of evidence therefore
589 support the conclusion that DSW is not produced in the DP: DSW has never been
590 observed on the shelf, sea-ice production is lower compared to polynyas where DSW is
591 produced, glacial meltwater that acts to weaken DSW production [*Williams et al.*, 2016]
592 is widespread and some observations during the past 20 years show that WW is much
593 fresher than the underlying mCDW, indicating weak salinification in wintertime.
594 The similarities of the ocean properties in 1996, 2007 and 2015 coupled with the
595 limited interannual changes in sea-ice production suggest that the marginal role of the DP
596 in setting the mCDW properties on the continental shelf observed in 2015 is
597 representative. Modelling studies suggest that cold water originated in the polynya mixes

with warm mCDW before entering in contact with the ice shelves. This process limits the ice-shelf basal melt, especially in years when the polynya is more active [*Khazendar et al.*, 2013; *Gwyther et al.*, 2014]. In light of our results this mechanism seems unlikely to play a primary role. We note, however, that more oceanographic data in the DP able to resolve the interannual variability of the evolution of the winter mixed layer are required to unequivocally assess the validity of this inference.

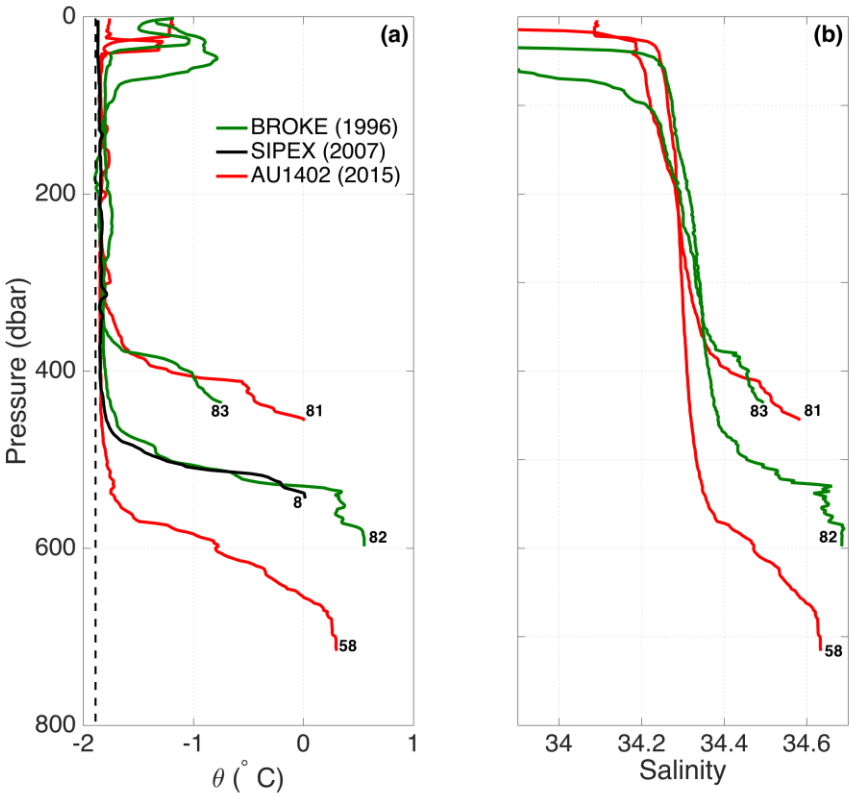

Figure 10. SIPEX-BROKE-AU1402. Vertical profiles of (a) potential temperature θ and (b) salinity from BROKE in 1996 (dark green, station 82-83) and SIPEX in 2007 (black, station 8). For comparison two profiles from AU1402 in 2015, one from the northern DP (station 81) and one from the western DP (station 58), are overlaid in red. In (a) overlaid in dashed black is the surface freezing temperature for a salinity of 34.4, representative of the domain. The location of the stations is labelled in Figure 1. Salinity data from SIPEX presented a large offset (>0.1) and therefore are not included here.

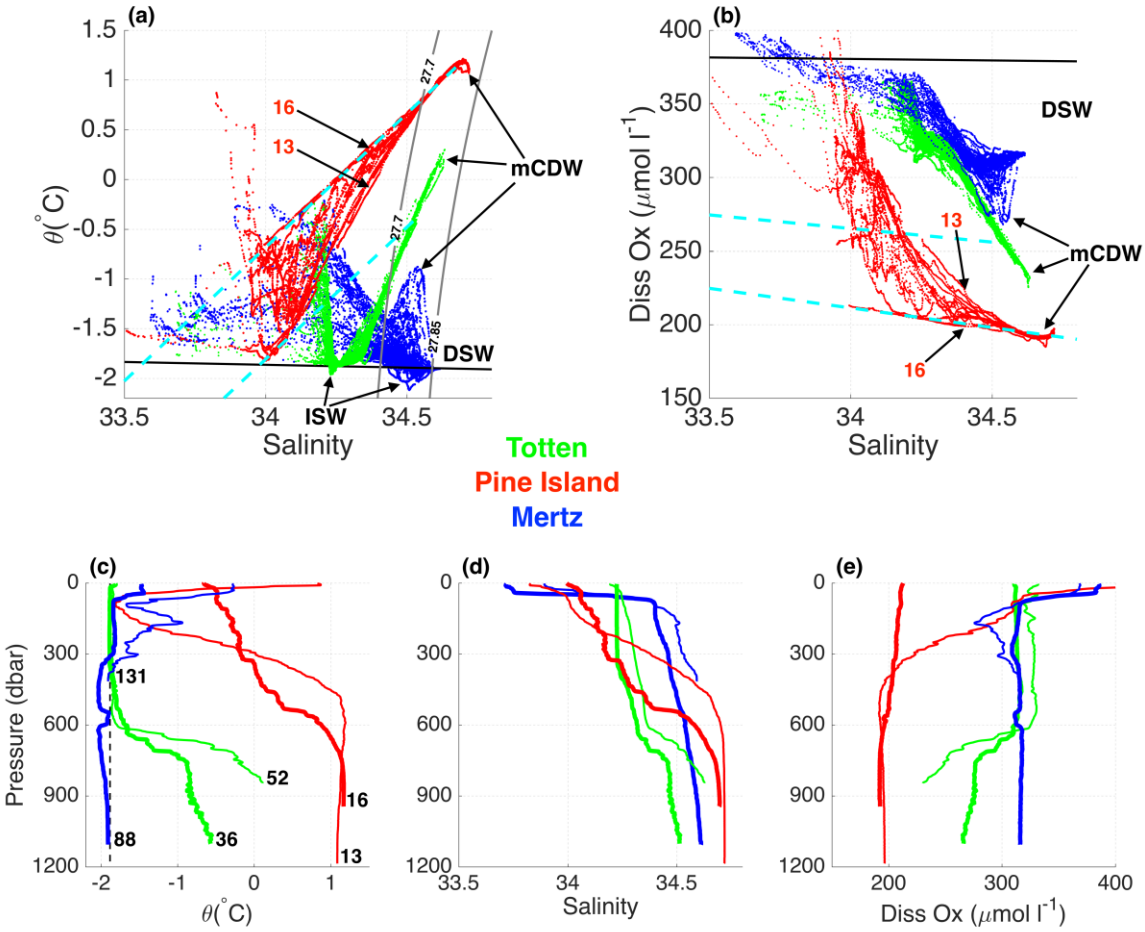

Figure 11. Comparisons between Totten, Mertz and Pine Island glaciers. (a) Potential temperature θ versus salinity from the shelf in front of Totten (green), Mertz (blue) and Pine Island (red) glaciers. The grey lines represent the surface of σ_θ = 27.7 kg m^{-3} (upper boundary of mCDW) and σ_θ = 27.85 kg m^{-3} (upper boundary of DSW). The black line is the surface freezing point. The cyan dashed lines are the mixing line between the warmest mCDW found in front of Totten/Pine Island and pure glacial meltwater. (b) As (a) for dissolved oxygen versus salinity. The black line indicates the surface of saturation for water at the surface freezing point. Vertical profiles of (c) θ, (d) salinity, (e) dissolved oxygen showing two profiles for each region. The thin lines are profiles representative of the shelf conditions (station 52/13/131 for Totten/Pine Island/Mertz). The thick lines are profiles representative of the ice-front conditions (station 36/16/88 for Totten/Pine Island/Mertz). The vertical dashed line in panel (c) indicates the surface freezing line for a salinity of 34.3, an intermediate value between the salinity observed at these three locations.

631 In order to contextualize our results, we compare the ocean properties observed
632 near the Totten Glacier with the Mertz Glacier on the Adélie Coast in East Antarctica and
633 with Pine Island Glacier in Pine Island Bay, West Antarctica (Figure 11). The mCDW is
634 found on each shelf, but with different properties. The warmest mCDW is observed in
635 Pine Island Bay (3-4°C above the in situ freezing point). On the Sabrina Coast the
636 mCDW is colder, but still 2-2.5°C above the local freezing point, while on the Adélie
637 Coast the mCDW is less than 1.3°C above the local freezing point. The ocean
638 stratification is similar on the Totten shelf (see station 52) and in Pine Island Bay (see
639 station 13): beneath the summer mixed layer, cold and fresh WW overlies warm, salty
640 mCDW. In contrast, on the Adélie Coast, the densest water is cold and oxygen rich DSW
641 formed during winter [*Shadwick et al.*, 2013] (for our work we consider the σ_θ=27.85 kg
642 m^{-3} isopycnal as the upper boundary of DSW). Above the DSW we find the mCDW, a
643 thin remnant of the WW layer and the summer mixed layer (see station 131). Intrusions
644 of mCDW are not dense enough to erode the DSW on the Adélie Coast, and as a result
645 the temperature maximum associated with mCDW is found at intermediate depth. In
646 Figure 12 we show a schematic of the different stratification found on the Sabrina Coast
647 and Pine Island Bay, and on the Adélie Coast.
648 The difference in stratification found in front of Totten/Pine Island and Mertz
649 glaciers is critical for the impact of the ocean on the ice shelf. Near the Mertz Glacier
650 relatively warm mCDW is found at depths shallower than 300 m and so has limited
651 access to the cavity beneath the Mertz Glacier Tongue. Cold DSW fills the cavity and
652 drives basal melt at depth. The cold and high oxygen ISW at the calving front (e.g.,
653 station 88) confirms that high oxygen DSW is the main source of melting under the

Mertz Tongue. High oxygen ISW is not found in front of Totten and Pine Island glaciers because the melting source is the low oxygen mCDW. The last important difference between the Adélie Coast and Sabrina Coast/Pine Island Bay is the freshness of the WW of the latter (~34.5-34.6 vs ~ 34.3/34). Fresh WW as a result of weak winter salinification is a key factor controlling the ocean influence on the ice sheet: weak convection in West Antarctica and near the Totten Glacier fosters rapid ice shelf basal melt by deep intrusions of warm waters, while strong heat loss and deep convection on several continental shelves in East Antarctica "protects" outlet glaciers by limiting the tranpsort of ocean heat to the cavity.

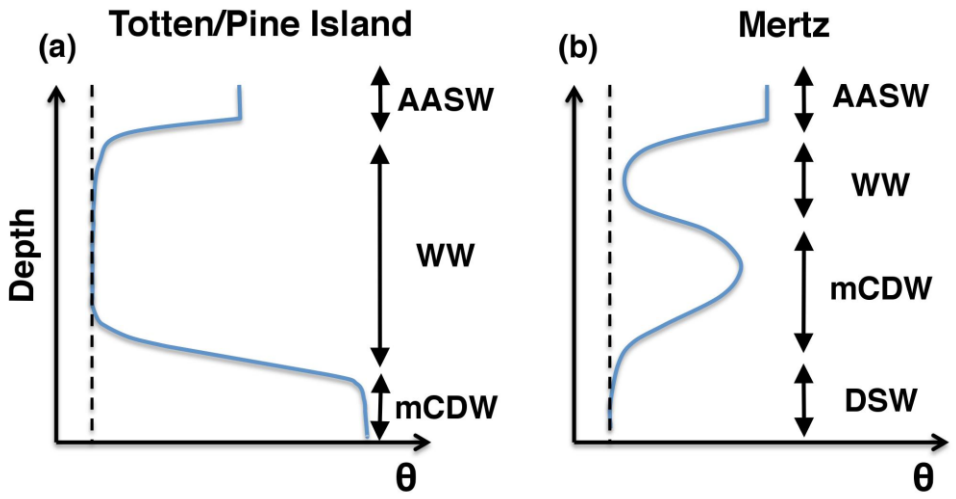

Figure 12. Schematic of the ocean summertime stratification in potential temperature θ in front of (a) Totten/Pine Island Glacier and (b) Mertz Glacier. AASW = Antarctic Surface Water; WW = Winter Water; mCDW = modified Circumpolar Deep Water; DSW = Dense Shelf Water.

672 The continental shelves on the Sabrina Coast and in West Antarctica share several
673 characteristics: absence of DSW formation, similar stratification, high basal melt rates of
674 coastal ice shelves and widespread glacial meltwater at intermediate depths. There are
675 also some important differences. As mentioned before, the mCDW on the continental
676 shelf is warmer in Pine Island Bay than on the Sabrina Coast continental shelf. We note
677 that our data show the warmest mCDW is found in the deep water west of the polynya,
678 suggesting we may not have sampled the warmest waters found on the Sabrina Coast.
679 WW is fresher near Pine Island Glacier. At the calving front, basal meltwater
680 concentration of the outflow from the TIS cavity is ~ 30% of the values estimated from
681 Pine Island Glacier during the last 20 years [*Jacobs et al.,* 2011]. The higher meltwater
682 content near Pine Island Glacier is apparent in the θ-S and O-S diagram by the
683 overlapping of some measurements at the calving front with the mCDW-glacial
684 meltwater mixing line (see station 16). This overlapping is not observed at the Totten
685 Glacier presumably for two reasons. First, meltwater at the calving front may have
686 already mixed with WW. Second, the major outflow from the cavity may occur in the
687 westernmost sector of the TIS front (where fast ice prevented access during the survey).
688 The access of relatively warm water to the TIS and MUIS cavities through
689 localized troughs is not observed at Pine Island Glacier, where mCDW intrusions are
690 observed all along the calving front. Our results suggest that the primary mechanism that
691 regulates the thermal forcing of intrusions into the TIS and MUIS cavity is the pycnocline
692 depth on the continental shelf. If the pycnocline shoals, more mCDW may overcome any
693 physical barrier blocking access to the ice front, allowing warmer and more extensive
694 intrusions into the ice-shelf cavities and an increase in the rate of basal melt. On the

695 contrary, if the pycnocline deepens cooler intrusions would reduce the basal melt. Several
696 mechanisms can influence the depth of the pycnocline on the continental shelf.
697 Variability of mCDW intrusions onto the shelf can modify the thickness of the bottom
698 layer and the maximum depth of overlying pycnocline [*Thoma et al.*, 2008]. Local
699 changes in winds associated with upwelling/downwelling variability or
700 increseased/decreased freshwater fluxes from ice-shelf basal melt can also cause
701 substantial changes in the pycnocline depth [*Padman et al.,* 2012]. Finally, variability in
702 the winter convection and thus in the mixed layer thickness can alter the depth at which
703 the pycnocline starts. In this case polynya variability might be important, especially for
704 the nearby MUIS where our observations show that the mCDW core does not access the
705 cavity but only waters coming from the upper pycnocline. Therefore, deepening of the
706 upper pycnocline would prevent relatively warm water from reaching the ice shelf.
707 Winter convection depends on several processes such as winds, air temperature,
708 incoming longwave/shortwave radiation and air humidity [*Petty et al.,* 2013]. However,
709 the lack of consensus on future changes of these parameters [*Kusahara and Hasumi*,
710 2013] undermines our ability to fully predict on the Sabrina Coast (and in general on
711 every Antarctic continental shelf) the ocean heat flux to the outlet glaciers in the coming
712 decades and centuries.

713 Based on our snapshot, we show that ocean conditions on the Sabrina Coast
714 continental shelf resemble those of West Antarctica: warm mCDW is found in the bottom
715 layer beneath fresh surface waters and meltwater by melting ice shelves is widespread at
716 mid-depths on the inner shelf. In contrast to West Antarctica, access of relatively warm
717 water to the TIS and MUIS cavity is limited to a few deep troughs, reducing the potential

ocean heat flux to the base of the ice shelves. We note, however, that a complete assessment of the impact of the ocean on the glacial ice in this region requires several knowledge gaps to be filled. First of all, the bathymetry of this region is still poorly known and the pathway of warm water to the glaciers is unresolved. No measurements of the interannual variability of ocean heat flux to the cavities have been made and even less is known about the heat flux reaching the grounding line. And last, data from the calving front of the main and fast flowing trunk of MUIS are absent. Therefore we are not able to confirm if warm mCDW can also affect this area of the ice shelf. For these reasons further surveys are required to fully understand the ice-ocean processes involved in this critical region of Antarctica.

5. Conclusions

The oceanographic data collected in the austral summer of 2015 provide the most comprehensive hydrographic survey of the Sabrina Coast continental shelf to date. In most of the region covered by our survey we find warm mCDW in the bottom layer below fresh Winter Water. Glacial meltwater is widespread at mid-depths on the southern shelf. These features are atypical for East Antarctica but rather resemble those observed during the last two decades in West Antarctica, where the strong ice-sheet retreat has been linked to intrusions of mCDW into the ice-shelf cavities.

Our findings indicate that warm water drives rapid ice shelf basal melt on the Sabrina Coast, but its access to the cavities is restricted to narrow troughs. However, future changes in the pycnocline depth may change this condition, allowing warmer and more extensive intrusions of mCDW into the ice shelf cavities, enhancing the basal melt.

A collapse of the Totten Ice Shelf could initiate a rapid ice loss in the Aurora Basin in the next centuries affecting the global sea level by several meters [*Golledge et al.,* 2015; *DeConto and Pollard*, 2016]. Our observations suggest that changes of the ocean conditions on the Sabrina Coast could further increase the present ocean heat flux, possibly affecting the mass balance of the Totten Ice Shelf. It is therefore critical to monitor and improve our understanding of the processes regulating the ice-ocean interaction on the Sabrina Coast in order to predict the future behaviour of the outlet glaciers that drain through this region.

Acknowledgments

We thank the scientists, technicians, officers, and crew that participated to the RV *Aurora Australis* Expedition. The work was supported by the Australian Antarctic Research Program, the Australian Research Council's Special Research Initiative for the Antarctic Gateway Partnership, the Australian Climate Change Science Program, the Australian Government's Cooperative Research Centres Program through the Antarctic Climate & Ecosystems Cooperative Research Centre (ACE CRC) and the Australia's Integrated Marine Observing System. Alessandro Silvano is supported by the Australian Government through the Australian Postgraduate Awards (APA) and the International Postgraduate Research Scholarships (IPRS) and by CSIRO and University of Tasmania through the Quantitative Marine Science PhD program. We want to thank Jason Roberts (Australian Antarctic Division, ACE CRC) and Felicity Graham (University of Tasmania) for helpful discussions during the development of this work. Data are available from the Australian Antarctic Data Centre (https://data.aad.gov.au/).

References

Bindoff, N. L., M. A. Rosenberg, and M. J. Warner (2000), On the circulation and water masses over the Antarctic continental slope and rise between 80 and 150°E, *Deep Sea Res., Part II*, *47*(12-13), 2299–2326, doi:10.1016/S0967-0645(00)00038-2.

DeConto, R. M., and D. Pollard (2016), Contribution of Antarctica to past and future sea-level rise, *Nature*, *531*(7596), 591–597, doi:10.1038/nature17145.

Depoorter, M. A., J. L. Bamber, J. A. Griggs, J. T. M. Lenaerts, S. R. M. Ligtenberg, M. R. van den Broeke, and G. Moholdt (2013), Calving fluxes and basal melt rates of Antarctic ice shelves, *Nature*, *502*(7469), 89–93, doi:10.1038/nature12567.

Dupont, T. K., and R. B. Alley (2005), Assessment of the importance of ice-shelf buttressing to ice-sheet flows, *Geophys. Res. Lett.*, *32*, L04503, doi:10.1029/2004GL022024.

Dutrieux, P., J. De Rydt, A. Jenkins, P. R. Holland, H. K. Ha, S. H. Lee, E. J. Steig, Q. H. Ding, E. P. Abrahamsen, and M. Schroder (2014), Strong Sensitivity of Pine Island Ice-Shelf Melting to Climatic Variability, *Science*, *343*(6167), 174–178, doi:10.1126/science.1244341.

Foldvik, A., and T. Kvinge (1974), Conditional instability of sea-water at freezing-point. *Deep Sea Res.*, *21*(3):169–174.

Fretwell, P., et al. (2013), Bedmap2: Improved ice bed, surface and thickness datasets for Antarctica, *The Cryosphere*, *7*, 375–393, doi:10.5194/tc-7-375-2013.

Fyke, J. G., L. Carter, A. Mackintosh, A. J. Weaver, and K. J. Meissner (2010), Surface melting over ice shelves and ice sheets as assessed from modeled surface air temperatures, *J. Clim.*, *23*(7), 1929–1936, doi:10.1175/2009JCLI3122.1.

Gade, H. G. (1979), Melting of ice in sea water: A primitive model with application to the Antarctic ice shelf and icebergs, *J. Phys. Oceanogr.*, *9*, 189–198.

Gill, A. E. (1973), Circulation and bottom water production in the Weddell Sea, *Deep Sea Res. Oceanogr. Abstr.*, *20*(2), 111–140.

Golledge, N. R., D. E. Kowalewski, T. R. Naish, R. H. Levy, C. J. Fogwill, and E. G. W. Gasson (2015), The multi-millennial Antarctic commitment to future sea-level rise, *Nature*, *526*(7573), 421–425, doi:10.1038/nature15706.

800 Greenbaum, J. S., et al. (2015), Ocean access to a cavity beneath Totten Glacier in East
801 Antarctica, *Nat. Geosci.*, *8*(4), 294–298., doi:10.1038/ngeo2388.
802 Gwyther, D. E., B. K. Galton-Fenzi, J. R. Hunter, and J. L. Roberts (2014), Simulated
803 melt rates for the Totten and Dalton ice shelves, *Ocean Sci.*, *10*, 267–279,
804 doi:10.5194/os10-267-2014.
805 Harig, C., and F. J. Simons (2015), Accelerated West Antarctic ice mass loss continues to
806 outpace East Antarctic gains, *Earth Planet. Sci. Lett.*, *415*, 134–141,
807 doi:10.1016/j.epsl.2015.01.029.
808 Hellmer, H. H., S. S. Jacobs, and A. Jenkins (1998), Oceanic erosion of a floating
809 Antarctic glacier in the Amundsen Sea, in *Ocean, Ice, and Atmosphere:*
810 *Interactions at the Antarctic Continental Margin, Antarct. Res. Ser.*, vol. 75,
811 edited by S. S. Jacobs and R. F. Weiss, pp. 83–99, AGU, Washington, D. C.
812 Jacobs, S. S., A. F. Amos, and P. M. Bruchhausen (1970), Ross Sea oceanography and
813 Antarctic bottom water formation, *Deep Sea Res. Oceanogr. Abstr.*, 17(6), 935–
814 962.
815 Jacobs, S. S., H. H. Hellmer, C. S. M. Doake, A. Jenkins, and R. M. Frolich (1992),
816 Melting of ice shelves and the mass balance of Antarctica, *J. Glaciol.*, *38*(130),
817 375–387.
818 Jacobs, S. S., A. Jenkins, C. F. Giulivi, and P. Dutrieux (2011), Stronger ocean
819 circulation and increased melting under Pine Island Glacier ice shelf, *Nat.*
820 *Geosci.*, *4*(8), 519–523, doi:10.1038/ngeo1188.
821 Jacobs, S., C. Giulivi, P. Dutrieux, E. Rignot, F. Nitsche, and J. Mouginot (2013), Getz
822 Ice Shelf melting response to changes in ocean forcing, *J. Geophys. Res. Oceans*,
823 *118*, 4152–4168, doi:10.1002/jgrc.20298.
824 Jenkins, A. (1999), The impact of melting ice on ocean waters, *J. Phys. Oceanogr.*, *29*,
825 2370–2381.
826 Jenkins, A., and S. S. Jacobs (2008), Circulation and melting beneath George VI ice
827 shelf, Antarctica, *J. Geophys. Res.*, *113*, C04013, doi:10.1029/2007JC004449.
828 Johnson, G. C. (2008), Quantifying Antarctic Bottom Water and North Atlantic Deep
829 Water volumes, *J. Geophys. Res.*, 113, C05027, doi:10.1029/2007JC004477.
830 Khazendar, A., M. P. Schodlok, I. Fenty, S. R. Ligtenberg, E. Rignot, and M. R. van den

831 Broeke (2013), Observed thinning of Totten Glacier is linked to coastal polynya
832 variability, *Nat. Commun.*, *4*, 2857, doi:10.1038/ncomms3857.
833 Kim, I., D. Hahm, T. S. Rhee, T. W. Kim, C.-S. Kim, and S.H. Lee (2016), The
834 distribution of glacial meltwater in the Amundsen Sea, Antarctica, revealed by
835 dissolved helium and neon, *J. Geophys. Res. Oceans*, *121*, 1654–1666,
836 doi:10.1002/2015JC011211.
837 Kitade, Y., et al. (2014), Antarctic Bottom Water production from the Vincennes Bay
838 Polynya, East Antarctica, *Geophys. Res. Lett.*, *41*, 3528–3534,
839 doi:10.1002/2014GL059971.
840 Kusahara, K., and H. Hasumi (2013), Modeling Antarctic ice shelf responses to future
841 climate changes and impacts on the ocean, *J. Geophys. Res. Oceans*, *118*, 2454–
842 2475, doi:10.1002/jgrc.20166.
843 Li, X., E. Rignot, M. Morlighem, J. Mouginot, and B. Scheuchl (2015), Grounding line
844 retreat of Totten Glacier, East Antarctica, 1996 to 2013, *Geophys. Res. Lett.*, *42*,
845 8049–8056, doi:10.1002/2015GL065701.
846 Li, X., E. Rignot, J. Mouginot, and B. Scheuchl (2016), Ice flow dynamics and mass loss
847 of Totten Glacier, East Antarctica from 1989 to 2015, *Geophys. Res. Lett*., *43*,
848 6366–6373, doi:10.1002/2016GL069173.
849 Liu, Y., J. Moore, X. Cheng, R. Gladstone, J. Bassis, H. Liu, J. Wen, and F. Hui (2015),
850 Ocean-driven thinning enhances iceberg calving and retreat of Antarctic ice
851 shelves, *Proc. Natl. Acad. Sci. U.S.A.*, *112*, 3263–3268,
852 doi:10.1073/pnas.1415137112.
853 Marshall, J., and K. Speer (2012), Closure of the meridional overturning circulation
854 through Southern Ocean upwelling, *Nat. Geosci.*, *5*(3), 171–180,
855 doi:10.1038/ngeo1391.
856 Martinerie, P., D. Raynaud, D. M. Etheridge, J.-M. Barnola, and D. Mazaudier (1992),
857 Physical and climatic parameters which influence the air content in polar ice,
858 *Earth Planet. Sci. Lett., 112*, 1–13, doi:10.1016/0012-821X(92)90002-D.
859 Ohshima, K. I., et al. (2013), Antarctic Bottom Water production by intense sea-ice
860 formation in the Cape Darnley Polynya, *Nat. Geosci.*, *6*(3), 235–240,
861 doi:10.1038/ngeo1738.

862 Orsi, A. H., and C. L. Wiederwohl (2009), A recount of Ross Sea waters, *Deep Sea Res.*,
863 *Part II*, *56*, 778–795, doi:10.1016/j.dsr2.2008.10.033.
864 Padman, L., et al. (2012), Oceanic controls on the mass balance of Wilkins Ice Shelf,
865 Antarctica, *J. Geophys. Res.*, *117*, C01010, doi:10.1029/2011JC007301.
866 Paolo, F. S., H. A. Fricker, and L. Padman (2015), Volume loss from Antarctic ice
867 shelves is accelerating, *Science*, *348*(6232), 327–331,
868 doi:10.1126/science.aaa0940.
869 Petty, A. A., D. L. Feltham, and P. R. Holland (2013), Impact of atmospheric forcing on
870 Antarctic continental shelf water masses, *J. Phys. Oceanogr.*, *9*, 920–940, doi:
871 10.1175/JPO-D-12-0172.1.
872 Picard, G., and M. Fily (2006), Surface melting observations in Antarctica by microwave
873 radiometers: Correcting 26-year time series from changes in acquisition hours,
874 *Remote Sensing Environ., 104*(3), 325–336, doi:10.1016/j.rse.2006.05.010.
875 Pritchard, H. D., S. R. M. Ligtenberg, H. A. Fricker, D. G. Vaughan, M. R. van den
876 Broeke, and L. Padman (2012), Antarctic ice–sheet loss driven by basal melting
877 of ice shelves, *Nature*, *484*(7395), 502–505, doi:10.1038/nature10968.
878 Randall-Goodwin, E., et al. (2015), Freshwater distributions and water mass structure in
879 the Amundsen Sea Polynya region, Antarctica, *Elem. Sci. Anthr.*, *3*(1), 000065,
880 doi:10.12952/journal.elementa.000065.
881 Rignot, E., J. L. Bamber, M. R. van den Broeke, C. Davis, Y. Li, W. J. van de Berg, and
882 E. van Meijgaard (2008), Recent Antarctic ice mass loss from radar
883 interferometry and regional climate modelling, *Nat. Geosci.*, *1*, 106–110,
884 doi:10.1038/ngeo102.
885 Rignot, E., S. Jacobs, J. Mouginot, and B. Scheuchl (2013), Ice-shelf melting around
886 Antarctica, *Science*, *341*(6143), 266–270, doi:10.1126/ science.1235798.
887 Rintoul, S. R. (1998), On the origin and influence of Adélie Land Bottom Water, in
888 *Ocean, Ice, Atmosphere: Interactions at the Antarctic Continental Margin,*
889 *Antarct. Res. Ser.*, vol. 75, edited by S. S. Jacobs and R. F. Weiss, pp. 151–171,
890 AGU, Washington, D. C.
891 Rintoul 2016
892 Rosenberg, M., and S. R. Rintoul (2016), Aurora Australis marine science cruise

AU1402, Totten and Mertz CTDs and moorings – oceanographic field measurements and analysis. ACE Cooperative Research Centre, May 2016, unpublished report, 69 pp.

Scambos, T., J. Bohlander, and B. Raup (1996), *Images of Antarctic Ice Shelves [January 2015]*, Boulder, Colorado USA: National Snow and Ice Data Center, http://dx.doi.org/10.7265/N5NC5Z4N.

Shadwick, E. H., S. R. Rintoul, B. Tilbrook, G. D. Williams, N. Young, A. D. Fraser, H. Marchant, J. Smith, and T. Tamura (2013), Glacier tongue calving reduced dense water formation and enhanced carbon uptake, *Geophys. Res. Lett., 40,* 904–909, doi:10.1002/grl.50178.

Shepherd, A., D. Wingham, and E. Rignot (2004), Warm ocean is eroding West Antarctic Ice Sheet, *Geophys. Res. Lett.*, *31*, L23402, doi:10.1029/2004GL021106.

Smith, W. H. F., and D. T. Sandwell (1997), Global seafloor topography from satellite altimetry and ship depth soundings, *Science*, *277*, 1957–1962.

Sun, S., S. L. Cornford, D. E. Gwyther, R. M. Gladstone, B. K. Galton-Fenzi, L. Zhao, and J. C. Moore (2016), Impact of ocean forcing on the Aurora Basin in the 21st and 22nd centuries, *Ann. Glaciol.*, 1–8, doi: 10.1017/aog.2016.27.

Tamura, T., K. I. Ohshima, A. D. Fraser, and G. D. Williams (2016), Sea ice production variability in Antarctic coastal polynyas, *J. Geophys. Res. Oceans*, *121*, 2967–2979, doi:10.1002/2015JC011537.

Thoma, M., A. Jenkins, D. Holland, and S. Jacobs (2008), Modelling Circumpolar Deep Water intrusions on the Amundsen Sea continental shelf, Antarctica, *Geophys. Res. Lett.*, *35*, L18602, doi:10.1029/2008GL034939.

Wahlin, A., X. Yuan, G. Bjork, and C. Nohr (2010), Inflow of warm circumpolar deep water in the central Amundsen Shelf, *J. Phys. Oceanogr.*, *40*(6), 1427–1434., doi: 10.1175/2010JPO4431.1.

Williams, G. D., A. J. S. Meijers, A. Poole, P. Mathiot, T. Tamura, and A. Klocker (2011), Late winter oceanography off the Sabrina and BANZARE coast (117–128 E), East Antarctica, *Deep Sea Res., Part II, 58*(9-10), 1194–1210, doi:10.1016/j.dsr2.2010.10.035.

Williams, G. D., et al. (2016), The suppression of Antarctic bottom water formation by

melting ice shelves in Prydz Bay. *Nat. Commun.*, *7*, 12577, doi:10.1038/ncomms12577.

Wouters, B., A. Martin-Español, V. Helm, T. Flament, J. M. van Wessem, S. R. M. Ligtenberg, M. R. van den Broeke, and J. L. Bamber (2015), Dynamic thinning of glaciers on the Southern Antarctic Peninsula, *Science*, *348*(6237), 899–903, doi: 10.1126/science.aaa5727.

Zhang, X., A. F. Thompson, M. M. Flexas, F. Roquet, and H. Bornemann (2016), Circulation and meltwater distribution in the Bellingshausen Sea: From shelf break to coast, *Geophys. Res. Lett.*, *43*, 6402–6409, doi:10.1002/2016GL068998.